Towards Anti-Interference Human Activity Recognition Based on WiFi Subcarrier Correlation Selection

Jinyang Huang, Bin Liu, Chao Chen, Hongxin Jin, Zhiqiang Liu, Chi Zhang, and Nenghai Yu

***Abstract*—As an essential technology in the field of the Internet of Things, Human activity recognition (HAR) is a well-researched topic. Recently, some state-of-the-art WiFi-based HAR systems have been presented due to its characteristics of no-invasion, no privacy leakage, and high recognition accuracy rates (RARs). However, the commodity WiFi devices for identification are usually in a complex electromagnetic environment, where the interference caused by WiFi devices from channel overlap is common and severe. Furthermore, our extensive experiments show that the performance of these pioneer WiFi-based HAR systems may degrade significantly in co-channel interference (CCI) scenarios. To solve the above problem, we propose WiAnti, a WiFi-based HAR system that is robust to CCI. Two adaptive subcarrier selection algorithms, WiAnti-Pearson and WiAnti-DTW, are proposed to mitigate the impact of CCI and to improve the recognition performance in CCI scenarios. As demonstrated in the experimental results, WiAnti-Pearson yields a 95% RAR on average, which can improve up to a 14% RAR in the presence of constant CCI. Moreover, WiAnti-DTW achieves an 8% higher RAR in the varying CCI scenario, reaching 94%.**

***Index Terms*—WiFi CSI, human activity recognition (HAR), co-channel interference, anti-interference.**

I. Introduction

HUMAN activity recognition (HAR) systems have inspired novel user interfaces and new applications in smart cities, surveillance, and military missions [1]. To perform HAR in various situations, camera-based [2], [3] and sensor-based [4], [5] HAR schemes have been well studied in the literature. However, these traditional methods have several problems, such as privacy leaks, low recognition accuracy rates (RARs), and bad user experience [6].

For camera-based HAR systems, such as KVMD [2], and DSTIP [3], they are usually equipped with high-resolution cameras to record body movements and classify these records into different activities. These camera-based HAR systems can obtain high RARs. However, the environment condition has a significant effect on its recognition performance, and the privacy problem limits the scope of its applications. As for sensor-based HAR systems, multiple sensors attached to the body can monitor the motion information of different body parts, and then signal processing technology and classification technology are adopted to classify the current activity accordingly [4], [5]. However, they need to perform the prior professional calibration by experts before working well, and the additional equipment attached to the body downgrades the user experience.

In recent years, with the rapid development in wireless techniques, several device-free approaches, such as dedicated radio frequency (DRF)-based methods and WiFi-based methods, have attracted more and more attention [7]–[11]. Their key advantages over camera-based and sensor-based methods are that they do not require lighting, preserve user privacy, and do not require users to carry any devices. Specifically, DRF-based HAR systems basically employ the dedicated equipment, e.g., software defined radio (SDR) and universal software radio peripheral (USRP), to capture the channel frequency responses (CFR) of signals and measure these CFR changes reflected by the human body to recognize distinct activities [12], [13]. The performance of DRF-based systems is always satisfactory. However, these systems cannot realize dual purposes, i.e., communication and HAR, at the same time. Moreover, the DRF equipment is necessary and irreplaceable, but the price of the equipment is usually high. WiFi-based HAR systems can utilize off-the-shelf WiFi devices without adopting other specialized equipment to monitor the activities in the Area of Interest (AoI). One sending WiFi device and one receiving WiFi device are placed in two different places of AoI, and the receiving WiFi device receives the regular signals from the sending WiFi device. Since the different activities have distinct effects on the received signals, the valid signal processing methods can recognize different activities accordingly based on the received WiFi signals.

WiFi-based HAR systems mainly utilize two different kinds of signals, the Received Signal Strength Indication (RSSI) [10], [11] and the Channel State Information (CSI) [7]–[9], to classify different motions. RSSI, as the average measured power of the received radio signal [14], is a kind of coarse-grained radio channel measurement, and the performance of RSSI-based systems is greatly affected by the link quality. In the complex environment, the multipath propagation causes the fluctuations

Manuscript received September 11, 2019; revised February 4, 2020; accepted April 12, 2020. Date of publication April 21, 2020; date of current version June 18, 2020. The review of this article was coordinated by Prof. J.-M. Chung. *(Corresponding author: Bin Liu.)*

Jinyang Huang, Bin Liu, Hongxin Jin, Zhiqiang Liu, Chi Zhang, and Nenghai Yu are with the CAS Key Laboratory of Electromagnetic Space Information, University of Science and Technology of China, Hefei 230026, China (e-mail: huangjy@mail.ustc.edu.cn; flowice@ustc.edu.cn; jhx0112@mail.ustc.edu.cn; lzhq28@mail.ustc.edu.cn; chizhang@ustc.edu.cn; ynh@ustc.edu.cn).

Chao Chen is with the Institute of Information Science and Electronic Engineering, Zhejiang University, Hangzhou 310027, China (e-mail: chench@zju.edu.cn).

Digital Object Identifier 10.1109/TVT.2020.2989322

of the link quality. Therefore, good performance cannot always be guaranteed [15]. Compared with RSSI, CSI is a fine-grained value derived from the physical layer of the WiFi device [8], which can reflect the channel frequency response to capture the signal phase and amplitude information of different subcarriers. More information can be extracted to capture a subtle change of the link quality. Therefore, CSI-based systems have better robustness to the complex environment.

Unfortunately, according to the channel assignment strategy of the IEEE 802.11n standard [16], the overlapped subcarriers exist in the adjacent five WiFi channels. Furthermore, multiple routers are usually placed in one place, and each router would randomly choose the channel for transmission. Thus, the occurrence of co-channel interference (CCI) is inevitable. Moreover, CCI also has severe negative impacts on WiFi signals, i.e., the reduction of packet number and the weaken of subcarrier correlation, which finally leads to the degradation of WiFi-based HAR system performance. In the literature, no researcher has addressed this problem. To overcome the problem, we propose a CSI-based HAR system, **WiAnti**, which can effectively classify various motions in CCI scenarios. The main contributions of this paper are expressed in three aspects:

- As far as we know, this work is the first to introduce the effect of CCI on WiFi-based HAR systems, and we propose a novel Anti-interference and Non-intrusive HAR System WiAnti leveraging CSI from a single commodity WiFi device.
- We propose two novel subcarrier selection algorithms, i.e., Pearson (Pearson Correlation Coefficient)-based and DTW (Dynamic Time Warping)-based algorithms to deal with various CCI scenarios. Instead of simply fusing subcarriers, these two algorithms dynamically select subcarriers according to their correlation changes. We show that these two algorithms can select subcarriers with more motion information and outperform the state-of-the-art subcarrier fusion algorithms while reducing the data dimension.
- Extensive experiments of different CCI have been performed in various scenarios. The results of the experiments show that WiAnti achieves a 95% RAR on average in the various CCI scenarios and obtains an 11% higher RAR on average than the pioneer solutions.

The rest of the paper is organized as follows. Section II introduces the related works. Section III presents background materials on CSI and the impact of CCI on CSI. Then, in Section IV, a CSI-based HAR system WiAnti is proposed, and two subcarrier selection algorithms, WiAnti-Pearson and WiAnti-DTW, are introduced accordingly. Next, the evaluation results through experiments, and the impact of various factors on different algorithm performance are presented in Section V. Section VI concludes the paper.

II. Related Work

According to the signal used for motion detection, existing device-free HAR systems can be grouped into three categories: DRF-based, RSSI-based, and CSI-based.

Generally, there are three requirements for device-free HAR systems, including informative measurements, universal, and robustness to interference.

- **Informative measurements**: Contain information to recognize activity accurately.
- **Universal**: Use existing equipment or deployable on off-the-shelf infrastructure.
- **Robustness to Interference**: Reduce or eliminate the effects of interference.

To summarize the pros and cons of different device-free HAR methods, a Venn diagram with the three features of informative measurements, universal, and robustness to interference is drawn in Fig. 2. This diagram is used to differentiate various approaches, and shows which solution can deal with which requirements.

A. DRF-Based Techniques

Fine-grained DRF measurements can be obtained by using dedicated hardware, such as SDR and USRP. The SDR was adopted to measure the received signal fluctuations, which were caused by the individual movement. Then, the speed of human walking was evaluated through the effective signal processing technology [12]. WiSee used USRP to capture the Orthogonal Frequency Division Multiplexing (OFDM) signals and measured the Doppler shift in signals reflected by bodies to recognize a set of nine different activities with a high RAR [17]. However, all of these schemes need dedicated hardware to achieve high RARs, which do not satisfy the universal requirement. Thus, DRF-based systems are expressed as a black circle in Fig. 2.

B. RSSI-Based Techniques

RSSI is an indication to measure the received signal power. Since different activities cause distinct RSSI fluctuations, activities can be recognized by processing the RSSI signals accordingly. PAWS designed an online HAR system, which explored WiFi ambient signals for RSSI fingerprint of different motions [10]. Wigest leveraged changes in WiFi RSSI to sense in-air hand gestures around the user's mobile device [11]. However, these approaches can only do coarse-grained HAR since RSSI falls entirely in the time domain, while frequency features are totally neglected. Suffering from performance degradation due to the multipath effect is also a problem for RSSI-based systems [15]. Thus, RSSI-based HAR systems are expressed as a green octagon in Fig. 2.

C. CSI-Based Techniques

Compared with RSSI, CSI is a fine-grained value derived from the physical layer of WiFi devices. In CSI-based systems, features are descriptions of motion from different perspectives, i.e., time domain and frequency domain. Frog Eye proposed a novel device-free crowd counting method based on CSI measurements [15]. E-eyes presented location-oriented activity identification, such as cooking and gaming [7]. WiShop analyzed shopper's behavior through WiFi signals [18]. WiFall-1 exploited the CSI

special diversity to detect human fall in an indoor environment and used the subcarrier fusion method for data dimension reduction [19]. Compared with WiFall-1, WiFall-2 used the subcarrier fusion method with frequency as a weight indicator [9]. However, most existing works do not consider the effects of CCI, and their experimental results are based on a non-CCI environment. Moreover, the performance of these systems degrades due to CCI. Thus, the traditional CSI-based methods are expressed as a blue diamond in Fig. 2. To overcome these drawbacks, we present WiAnti, a CSI-based HAR system that is robust to CCI. This means the proposed system WiAnti satisfies all three requirements.

III. Preliminaries and Observation

A. Overview of Channel State Information

In the frequency domain, the narrow-band flat-fading channel with multiple transmit and receive antennas (MIMO) can be modeled as [17]:

$$\boldsymbol{y}_i = \boldsymbol{H}_i \boldsymbol{x}_i + \boldsymbol{n}_i \tag{1}$$

where i denotes the stream corresponding to the i^{th} transmitter and receiver antenna (Tx-Rx) pair, and $\boldsymbol{x}_i$, $\boldsymbol{y}_i$ denote the transmitted and received signal vectors, respectively. $\boldsymbol{n}_i$ is the noise vector, and $\boldsymbol{H}_i$ is the channel matrix.

$\boldsymbol{H}_i$ can be estimated at the receiver when a known sequence is transmitted. As the IEEE 802.11n standard [16] is a protocol based on OFDM technology, the 2.4 to 2.4835 GHz band is divided into 14 channels, where each channel has 20M bandwidth, and there are 56 subcarriers in each channel. Therefore, the estimated value of $\boldsymbol{H}_i$ for N subcarriers can be represented as:

$$\boldsymbol{H}_i = [\boldsymbol{h}_i{}^{(1)}, \boldsymbol{h}_i{}^{(2)}, \ldots, \boldsymbol{h}_i{}^{(k)}, \ldots \boldsymbol{h}_i{}^{(N)}] \tag{2}$$

Since human bodies and surrounding objects reflect radio signals, a transmitted signal arrives at the receiver through multiple paths. If a wireless signal (k^{th} subcarrier in i^{th} Tx-Rx pair) arrives at the receiver through Υ different paths, $\boldsymbol{h}_i{}^{(k)}(\omega, t)$ can be given by the following equation [20], [21]:

$$\boldsymbol{h}_i{}^{(k)}(\omega, t) = e^{-j\cdot 2\pi\Delta\omega t} \sum_{\gamma=1}^{\Upsilon} \varphi_\gamma(\omega, t) \cdot e^{-j\cdot 2\pi\omega\tau_\gamma(t)} \tag{3}$$

where j is the imaginary unit, ω denotes the k^{th} subcarrier frequency, $\varphi_\gamma(\omega, t)$ denotes the complex-valued representation of attenuation and initial phase offset of the γ^{th} path, and $e^{-j\cdot 2\pi\omega\tau_\gamma(t)}$ is the phase shift on the γ^{th} path which has a propagation delay of $\tau_\gamma(t)$. Besides, $e^{-j\cdot 2\pi\Delta\omega t}$ is the phase shift caused by the subcarrier frequency difference between the transmitter and the receiver.

According to [20]–[22], the length changes of a path result in the phase change of the WiFi signal on the corresponding path. In particular, Fig. 1 shows that the subcarrier signal is reflected by the human body through the γ^{th} path. When the subject body moves by a small distance between time 0 and time t, the γ^{th} path length changes from $\vartheta_\gamma(0)$ to $\vartheta_\gamma(t)$. Since wireless signals travel at light speed c, the delay $\tau_\gamma(t)$ of the γ^{th} path can be

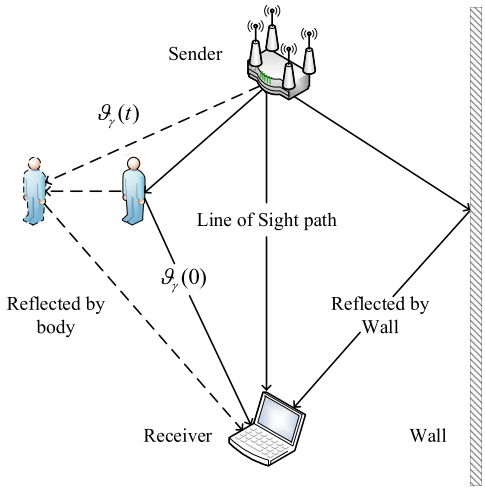

Fig. 1. Multipath caused by human movements.

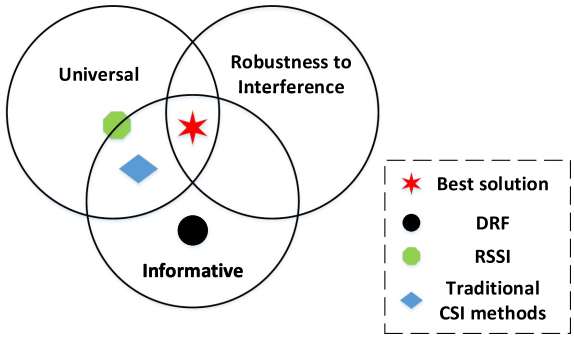

Fig. 2. Differentiating various approaches of device-free HAR systems.

expressed as $\tau_\gamma(t) = \vartheta_\gamma(t)/c$. Let λ represents the wavelength of k^{th} subcarrier, where $\lambda = c/\omega$. Consequently, the phase shift $e^{-j\cdot 2\pi\omega\tau_\gamma(t)}$ on this path can be rewritten as $e^{-j\cdot 2\pi\vartheta_\gamma(t)/\lambda}$, which clearly means that if the path length changes by one wavelength, the receiver experiences a phase shift of 2π in the corresponding received subcarrier. Furthermore, human movements change the phases of the different paths at the receiver and the number of multipath. Therefore, the different paths are superimposed according to the new phase relationship, which finally results in the fluctuations of corresponding subcarrier amplitudes [23].

In experiments, the subcarrier frequency response is measured by CSI collection tools [8], [24] and expressed as:

$$\boldsymbol{h}_i{}^{(k)} = \left|\boldsymbol{h}_i{}^{(k)}\right| \cdot e^{-j\cdot\theta_i{}^{(k)}} \quad k \in \boldsymbol{K} \tag{4}$$

where $|\boldsymbol{h}_i{}^{(k)}|$ and $\theta_i{}^{(k)}$ are the amplitude and the phase of the k^{th} subcarrier in the i^{th} Tx-Rx pair, respectively. $\boldsymbol{K}$ contains the subcarrier indexes. Although the WiFi system has 56 subcarriers over a 20 MHz channel, different NICs using distinct CSI collection tools [8], [24] can report the different number of subcarriers. For instance, the Intel 5300 using CSITOOL [8] can only report CSI for 30 of the 56 subcarriers, and the subcarrier index sequence $\boldsymbol{K}$ for Intel 5300 is $[-28, -26, \ldots, -2, -1, 1, 3, \ldots, 27, 28]$. To avoid misleading, we use the dictionary structure of $[key, value]$ to express the

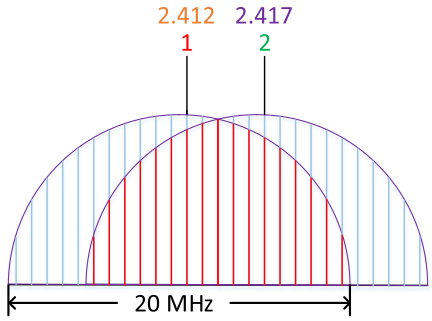

Fig. 3. Subcarriers overlap in adjacent channels.

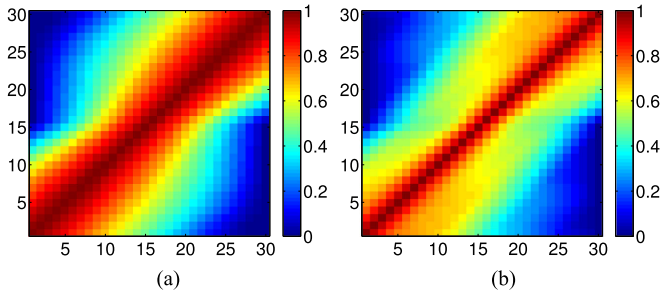

Fig. 4. Point correlation matrix of CSI subcarriers. (a) Point correlation without CCI. (b) Point correlation with CCI.

relationship between the key^{th} subcarrier reported by the corresponding CSI collection tool and the subcarrier $value$ in the IEEE 802.11n standard. In particular, $value = \boldsymbol{K}[key]$. For example, 15^{th} ($key = 15$) subcarrier in CSITOOL represents the subcarrier -1 ($\boldsymbol{K}[15] = -1$) in the IEEE 802.11n standard. In addition, unless otherwise specified, the experimental results in this paper are based on CSITOOL.

B. Impact of CCI on CSI

CCI is mainly caused by the nodes with the overlapped frequency spectrum competing for channels. According to the IEEE 802.11n standard [16], each channel contains 56 subcarriers in the 20MHz bandwidth. As long as the subcarriers of a channel used by one node overlap with the subcarriers of the channel used by another node in a nearby place, the CCI occurs. For example, Fig. 3 shows that there are spectrally-overlapped subcarriers between channel 1 and channel 2 as marked in red. Thus, if one node uses channel 1, and another node uses channel 2 in the same area, the CCI occurs.

To ensure the accuracy of data transmission in each wireless node, according to the IEEE 802.11n standard, a channel can only be used by one node when it is idle [16]. However, when CCI exists, the probability that the node senses an ongoing transmission becomes larger, and the number of delays increases, which results in a decrease in the received packet number per unit time. Besides, to synchronize the data transmitted by all subcarriers in one channel, all subcarriers in this channel must transmit simultaneously, and a node can send packets only when it detects that all the sub-channels of the working channel are idle [25]. Thus, a node needs to compete for all sub-channels in the working channel before sending packets. To improve the ability of nodes competing for channels, a more flexible subcarrier power allocation strategy is used in the WiFi system [16]. Specifically, for each node, since the subcarriers allocated more energy dominate channel competition [26] due to the increasing probability of other nodes sense busy on the corresponding sub-channels [27], the spectrally-overlapped subcarriers are allocated more power [28], [29]. On the contrary, less power is allocated to the subcarriers in non-overlapping areas. In this way, the ability of the node competing for the whole channel in CCI is improved. However, the unbalanced subcarrier power allocation strategy causes different power of subcarriers, which finally leads to the correlations across subcarriers weakened [30].

Fig. 4 shows the heatmap comparison between the subcarrier correlation matrices (empty room data) with and without CCI. Each element in the matrices corresponds to the correlation coefficient between two subcarriers' amplitudes in one sample point. Red and Blue represent the correlation coefficients of 1 and 0, respectively. Fig. 4(a) depicts the strong correlation between 30 subcarriers without CCI. When the number of interval subcarriers between two subcarriers is less than 14, the correlation coefficients can go beyond 0.9. However, CCI has a significant impact on the subcarrier correlation. Fig. 4(b) shows the correlation between the 30 subcarriers with CCI, compared with Fig. 4(a), the red covered area in Fig. 4(b) is a significantly thinner line, which shows that CCI weakens the correlation between subcarriers.

Unfortunately, most state-of-the-art systems such as WiShop [18], WiFall-1 [19], and WiFall-2 [9] rely on the strong correlation between subcarriers to perform data dimension reduction. These methods use one or several fused subcarriers, which are mean of all or some subcarrier amplitudes, to represent all subcarrier characteristics. However, when CCI exists, the correlation between subcarriers weakens. The fused subcarriers are not suitable to describe all subcarrier characteristics since the difference between various subcarriers is too significant. Thus, the performance of most pioneer systems [9], [18], [19] degrades due to CCI.

It is worth mentioning that, since the existence of Carrier Sense Multiple Access with Collision Avoid (CSMA/CA) [16], different nodes share the channel in a time-division manner [25], [27]. Thus, the degraded performance (the influence of CCI) is not caused by the direct collisions of the different WiFi signals. Specifically, the degraded performance of pioneer WiFi-based systems is caused by the loss of motion information during the data dimension reduction (subcarrier fusion) due to the weak subcarrier correlation. However, the data dimension reduction is necessary to trade off the accuracy and the computational complexity. Therefore, the influence of CCI on WiFi-based HAR systems is inevitable.

IV. System Design and Methodology

In this section, the activity set and the overall structure of the WiAnti system are introduced.

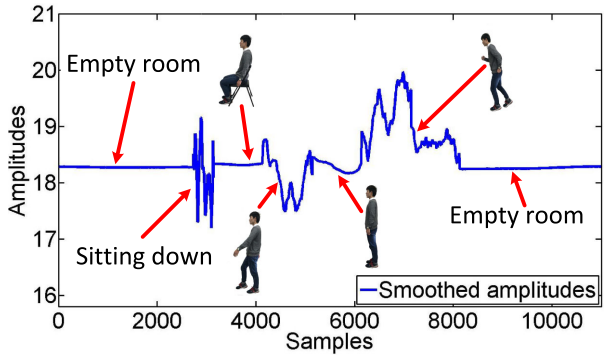

Fig. 5. The mean of the subcarrier CSI amplitude series for different activities in the activity set.

A. Activity Set Overview

We define one reference state, i.e., the empty room, and four regular motions, i.e., sitting, walking, standing, and running to find the impact of CCI in different situations. The sketch of each state or activity is shown in Fig. 5. A reference state of the empty room is set to evaluate the CCI in the background environment since we want to know how CCI affects the CSI signals without the influence of human motion. Fig. 5 also shows that the amplitude of CSI is a straight line with little variation when there are no people in the room. However, the fluctuations become significant when people are moving. Therefore, people's activities can be judged by the varying level of the CSI amplitude.

B. System Overview

As shown in Fig. 6, the workflow of the WiAnti system contains four main parts: judgment of CCI, adaptive data preprocessing, feature extraction, and classification part. The existence and the change of CCI are judged in the first part. Next, according to the judgment, different subcarrier processing strategies are adopted in the second part. Specifically, in the scenario without CCI, the data dimension is reduced by the usual subcarrier fusion method. On the contrary, in constant CCI scenarios, the Pearson-based subcarrier selection algorithm is used to improve the RAR. Moreover, the DTW-based subcarrier selection algorithm is adopted in varying CCI scenarios for further improvement of similar activity RARs. Then, the features are extracted in the third part. Finally, the activities are classified in the last part.

C. CCI Detection

Generally, CCI can be grouped into two categories: constant CCI and varying CCI.

As for constant CCI, the subcarrier correlation changes slowly due to fixed overlapped subcarriers and stable interference traffic rates (ITRs). Thus, it is easy to measure the subcarrier correlation. The local correlation features of sliding windows can well represent the global correlation characteristics of all samples due to the slowly changing subcarrier correlation. Based on the analysis, a Pearson-based algorithm is proposed to select subcarriers in constant CCI scenarios. The Pearson-based subcarrier selection algorithm tries to use the local correlation of sliding windows to represent the global correlation of all samples, which can measure subcarrier correlation effectively with low complexity.

Varying CCI usually happens when routers perform channel hopping or even when ITRs change. Different from constant CCI, the subcarrier correlation changes rapidly with varying CCI due to the change of overlapped subcarriers. Thus, the measurement of subcarrier correlation becomes more complicated, and the performance of the WiFi-based HAR system is limited. To improve the stability and representative of selected subcarriers and to further improve the RARs in varying CCI scenarios, a DTW-based subcarrier selection algorithm is proposed that can capture the global subcarrier correlation changes caused by varying CCI.

Besides, to perform appropriate subcarrier processing methods in corresponding CCI scenarios, the existence and the change of CCI need to be determined at first.

1) CCI Existence Detection: CCI is detected by recording the number of received packets per unit time. As introduced in Section III-B, in the scenario without CCI, the channel is only occupied by one node. The node sends packets as usual, and the number of received packets does not decrease per unit time. However, in CCI scenarios, the probability that the node senses an ongoing transmission becomes larger [27], and the number of delays increases, which leads to a decrease in the received packet number per unit time. Therefore, by recording the number of received packets per unit time, the existence of CCI is determined.

2) CCI Change Detection: Since spectrally-overlapped subcarriers and ITRs keep almost unchanged when CCI is constant, the node sends packets with the same delays in different unit time. Consequently, the fluctuation range of the received packet number per unit time is small. However, the fluctuation range becomes more significant when CCI is varying. Therefore, by observing the fluctuation level of received packet number per unit time, the state of CCI change can be judged. Specifically, if the fluctuation of the received packet number per unit time is within a threshold, the CCI is considered as unchanged in this scenario. Here, the state of CCI changing or not in each unit time is determined by using the following equations:

$$\frac{|P_m - P_{m-1}|}{P_{m-1}} < \sigma, \sigma > 0 \tag{5}$$

$$\overline{P} = \frac{\sum_{i=s}^{m-1} P_i}{m-1-s}, \frac{|P_m - \overline{P}|}{\overline{P}} < \xi, \xi > 0 \tag{6}$$

where P_m is the number of received packages in the m^{th} unit time, and σ and ξ are the thresholds corresponding to the two equations, respectively. Eq. (5) limits that the fluctuation between two adjacent unit time is less than a given threshold σ. Furthermore, Eq. (6) is supplementary for Eq. (5), which prevents the problem that the received packet number per unit time deviating from the normal threshold ξ in a gradually increasing or gradually decreasing manner, and still judged as CCI unchanged. Specifically, the fluctuation between the current

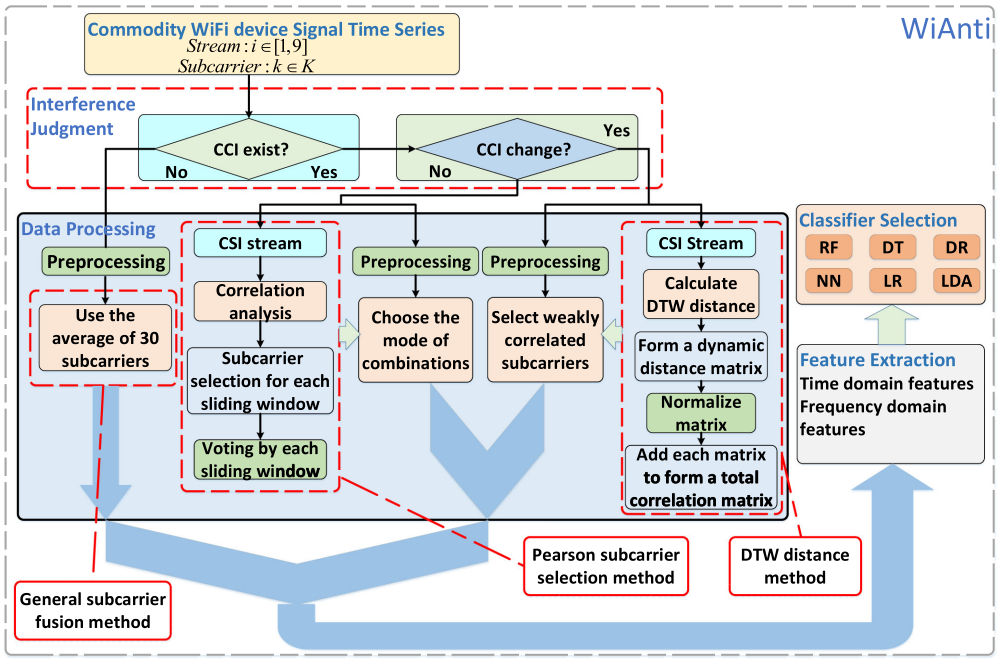

Fig. 6. WiAnti workflow.

unit (m^{th} unit) and the average of the previous units (s^{th} unit to $(m-1)^{th}$ unit in Eq. (6)), which are judged as CCI unchanged, is limited within a given threshold ξ. If the received packet number in m^{th} unit time satisfies these two equations, the CCI is regarded as unchanged in this unit.

D. Pearson-Based Subcarrier Selection Algorithm for Constant CCI Scenarios

Since each action takes place in several seconds, a moment (sample point) subcarrier correlation matrix (as shown in Fig. 4) may not fully reflect the correlation change during the motion. Compared with a single sample point, the sequence contains more time-domain information because it includes all the sampling points during the motion. Thus, the sequence correlation calculation methods are more representative of the subcarrier correlations during the movement.

As introduced in Section IV-C, WiAnti uses Pearson's method to calculate subcarrier sequence correlation in constant CCI scenarios.

The Pearson correlation coefficient [31] defines the strength of the correlation $r_{\boldsymbol{q},\boldsymbol{w}}$ using the covariance and standard deviation of two sequence variables ($\boldsymbol{q}$ and $\boldsymbol{w}$):

$$r_{\boldsymbol{q},\boldsymbol{w}} = \frac{\sum_{i=1}^{l}(q_i-\overline{q})(w_i-\overline{w})}{\sqrt{\sum_{i=1}^{l}(q_i-\overline{q})^2}\sqrt{\sum_{i=1}^{l}(w_i-\overline{w})^2}} \tag{7}$$

where l is the length of sequence $\boldsymbol{q}$ and sequence $\boldsymbol{w}$. $\overline{q}$ and $\overline{w}$ are the means of sequences $\boldsymbol{q}$ and $\boldsymbol{w}$, respectively. Specifically, in each sliding window of motion samples, sequences $\boldsymbol{q}$ and $\boldsymbol{w}$ represent the amplitude sequences of q^{th} subcarrier and w^{th} subcarrier in this sliding window, respectively. Thus, $r_{\boldsymbol{q},\boldsymbol{w}}$ represents the Pearson correlation coefficient between q^{th} subcarrier sequence and w^{th} subcarrier sequence in the corresponding sliding window.

In order to reduce the data dimension, most state-of-the-art works [7], [9], [11], [18], [19] used one or several fused subcarriers which are mean of some or all subcarrier amplitudes to represent the characteristics of all subcarriers. For instance, Wishop [18] used one fused subcarrier, which is a mean of 30 subcarrier amplitudes, to describe the features of all subcarriers. Besides, WiFall-1 [19] used six fused subcarriers to represent the features of all subcarriers. Each fused subcarrier in WiFall-1 is the mean of five adjacent subcarrier amplitudes. Different from WiFall-1, WiFall-2 [9] employed the subcarrier fusion method with subcarrier center frequency as a weight indicator. However, CCI makes these methods not as effective as they perform in a non-CCI environment. This is because CCI weakens the subcarrier correlation, and one can be represented by each other only when the two subcarriers are very similar. Therefore, it is unreasonable to represent all subcarrier characteristics with the fused subcarriers generated by these algorithms, which may perform unsatisfactorily due to CCI.

To better demonstrate that CCI weakens the subcarrier correlation, Fig. 7 depicts the heatmap comparison between the subcarrier sequence correlation matrices with and without CCI. Each element in the matrices corresponds to the correlation coefficient between two subcarrier amplitude sequences in one sliding window, and the sliding window data collected from the empty room to observe the impact of CCI on subcarrier correlation without motion effect. As shown in Fig. 7(a), the correlation between any two subcarrier sequences without CCI is strong, and the mean of its correlation coefficients calculated by Pearson's method can reach 0.85. Under such circumstances, it is reasonable to use the fused subcarrier features to represent the features of other subcarriers.

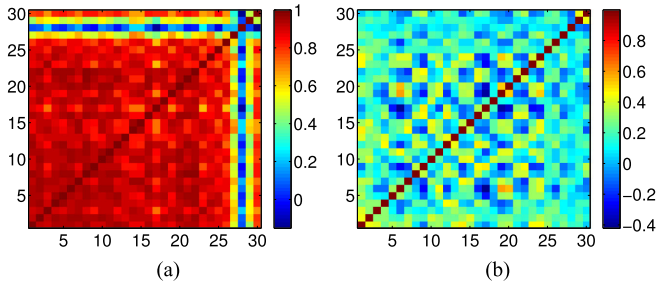

Fig. 7. Correlation matrix of subcarrier time sequences. (a) Sequence correlation without CCI. (b) Sequence correlation with CCI.

However, Fig. 7(b) depicts that the sequence correlation coefficients between any two subcarriers rarely reach 0.3 in the constant CCI scenario. Thus, it is unreasonable to use the subcarrier fusion algorithms [9], [18], [19] to perform the data dimension reduction due to the significant difference across distinct subcarriers.

Compared with the fusion algorithms [9], [18], [19], the subcarrier selection algorithms are more effective. Specifically, by selecting several weakly correlated subcarriers without subcarrier fusion to represent all subcarrier characteristics, the motion features can be retained at the maximum level with low complexity. This is because that weakly correlated subcarriers contain more information than the same number of strongly correlated subcarriers. According to information theory [32], the joint entropy can directly represent the amount of total information combined by two events. In particular, the joint entropy of two subcarrier sequences can be expressed as:

$$E(\boldsymbol{q}, \boldsymbol{w}) = E(\boldsymbol{q}) + E(\boldsymbol{w}) - \psi(\boldsymbol{q}; \boldsymbol{w}) \tag{8}$$

where $\boldsymbol{q}, \boldsymbol{w}$ are different subcarrier sequences. $E(\boldsymbol{q})$ and $E(\boldsymbol{w})$ are the entropy of subcarrier sequences $\boldsymbol{q}$ and $\boldsymbol{w}$, respectively. $E(\boldsymbol{q}, \boldsymbol{w})$ represents the joint entropy of subcarrier sequence $\boldsymbol{q}$ and subcarrier sequence $\boldsymbol{w}$. The mutual information $\psi(\boldsymbol{q}; \boldsymbol{w})$ is positively related to Pearson's correlation coefficient $r_{\boldsymbol{q},\boldsymbol{w}}$. Since $E(\boldsymbol{q})$ and $E(\boldsymbol{w})$ are invariant for given subcarrier sequences $\boldsymbol{q}$ and $\boldsymbol{w}$, the stronger correlation between the two subcarriers $\boldsymbol{q}, \boldsymbol{w}$, the bigger number of mutual information $\psi(\boldsymbol{q}; \boldsymbol{w})$, and the less information $E(\boldsymbol{q}, \boldsymbol{w})$ is contained.

Based on the above analysis, a Pearson-based dynamic subcarrier selection algorithm is employed in WiAnti to deal with constant CCI. The key idea of the Pearson-based algorithm is to select several weakly correlated subcarriers and not to fuse them. By using the features of the chosen subcarriers to represent all subcarrier characteristics, the data dimension is reduced with less information loss.

Three steps are included in the Pearson-based subcarrier selection algorithm:

Step 1: To maintain more motion information, the subcarrier combination with the weakest correlation in each sliding window of samples needs to be determined at first. Specifically, the inter-subcarrier correlation coefficients of f^{th} sliding window are calculated by Pearson's method to generate the correlation matrix R_f. The element $r_{\boldsymbol{q},\boldsymbol{w}}$ in R_f represents the coefficient of sequence correlation between the subcarrier sequence $\boldsymbol{q}$ and the subcarrier sequence $\boldsymbol{w}$. Then, all elements in the matrix R_f are sorted in an ascending order to generate a new array $\boldsymbol{I}_f$. Next, we choose the two subcarriers (a and b) with the minimum correlation coefficient value in array $\boldsymbol{I}_f$ to form the subcarrier combination C_f. Subcarriers are gradually added to the subcarrier combination C_f according to the weakest total correlation until the number of subcarriers in C_f reaches the given value o (the expected number of selected subcarriers). Similarly, we perform the same operation for all sliding windows. Thus, the subcarrier combinations of each sliding window are determined.

Step 2: To find a suitable subcarrier combination for all samples, step 2 is the effective screening of all subcarrier combinations. According to the principle of *minority subordinating to the majority*, the most frequently occurring subcarrier combination (the mode combination C_{tmp}) in all subcarrier combinations is chosen as the output of step 2. Thus, the global correlation characteristics of all samples are expressed by the local correlation features of sliding windows.

Step 3: Finally, as introduced in Section III-A, the farther interval between two subcarrier indexes causes the larger difference between subcarrier frequency ω, which finally leads to the more significant difference between these two subcarrier phase changes caused by the same motion. Thus, to balance the impact of the subcarrier phase change difference and the subcarrier correlation, the frequency spatial constraint of subcarriers is added in WiAnti algorithms. Specifically, subcarriers in the final chosen subcarrier combination C_s should be selected from all three subcarrier intervals, i.e., [0, 10), [10, 20), and [20,30]. If the output subcarrier combination of step 2 C_{tmp} does not satisfy this condition, the second most frequently occurring subcarrier combination is chosen. Similarly, if the second most frequently occurring subcarrier combination does not satisfy the condition, the third most frequently occurring subcarrier combination is chosen, and so on.

Algorithm 1 illustrates an algorithmic specification of the proposed Pearson-based subcarrier selection algorithm.

E. DTW-Based Subcarrier Selection Algorithm for Varying CCI Scenarios

The Pearson-based algorithm is particularly useful in constant CCI scenarios. Unfortunately, when CCI is varying, due to the unstable CSI collection tools [8], [24], the CSI of different subcarrier sequences appears more outlier values (exception values and zero values). To better reconstruct the real subcarrier sequences, we should better eliminate these outlier values accordingly. However, since these outlier values appear randomly in different subcarrier sequences, the numbers of outliers in different sequences are distinct, which results in the length difference between distinct subcarrier sequences after eliminating these outlier values. Unfortunately, the Pearson correlation calculation method can only measure the correlation between two equal-length sequences. Therefore, the Pearson correlation calculation method is unsuitable for CSI in varying CCI scenarios. Besides, the subcarrier correlation changes rapidly across different sliding windows due to the varying overlapped

Algorithm 1: Pearson-based Subcarrier Selection Algorithm.

Input: CSI streams (3×3), the length of each stream is L.

Output: The selected subcarrier combination C_s, which contain o subcarriers.

Initialize: The CSI stream is partitioned according to the sliding window size cw. Since there are 9 streams, the total number of sliding windows is $U = 9 \times \lfloor \frac{L}{cw} \rfloor$. Initialize B as an empty dictionary.
for $f <= U$, where f represents the f^{th} sliding window **do**
  $R_f =:$ the correlation matrix generated by calculating inter-subcarrier correlation coefficients according to Pearson's method.
  $\boldsymbol{I}_f :=$ the array generated by the arrangement of the elements in the matrix R_f from the smallest to largest order.
  According to $R_f(a, b) = \min(\boldsymbol{I}_f)$, selecting two subcarriers with the weakest correlation (a and b). At this point $C_f = \{a, b\}$.
  while $|C_f| <= o$ **do**
    $new =: \arg\ \min_{new}\{\sum_{i=1}^{|C_f|} r_{\boldsymbol{new},\boldsymbol{C_f}(i)}\}$.
    $C_f =: C_f \cup new$.
  end while
  if C_f in B **then**
    $B[C_f] = B[C_f] + 1$. // The key of the dictionary is the subcarrier combination, and the key value is the corresponding number of occurrences.
  else
    $B[C_f] = 1$.
  end if
  $f := f + 1$.
end for
while $B \neq \emptyset$ **do**
  $C_{tmp} := \arg\ \max_{C_w}\{B[C_w]\}$.
  if $C_{tmp} \cap [0, 10) \neq \emptyset$ and $C_{tmp} \cap [10, 20) \neq \emptyset$ and $C_{tmp} \cap [20, 30] \neq \emptyset$ **then**
    $C_s := C_{tmp}$.
    $break$.
  else
    del $B[C_{tmp}]$.
  end if
end while
return C_s.

subcarriers. The subcarrier combination selected by a single sliding window (the local correlation characteristics) cannot represent the correlation characteristics of all samples (the global correlation characteristics) well. Moreover, the final selected subcarrier combination C_s voted by all sliding windows is not prominent and not representative due to the significant difference between the various subcarrier combinations generated from different sliding windows. Therefore, an algorithm, which can measure the subcarrier correlation more accurately and precisely capture the correlation changes between different sliding windows, is needed to select representative subcarriers in varying CCI scenarios.

To deal with the above problems, a DTW-based algorithm is proposed to select the subcarriers in varying CCI scenarios. Different from the Pearson-based algorithm, the DTW-based algorithm employs DTW to calculate the subcarrier correlation since DTW can calculate the correlation between two subcarrier sequences with different lengths and is a more precise measurement of sequence correlation (the computational complexity of DTW increases accordingly). Furthermore, the DTW-based algorithm does not select subcarriers in each sliding window, but select subcarriers from the overall subcarrier correlation matrix which generated by adding subcarrier correlation matrices of all sliding windows. Thus, the DTW-based algorithm can better evaluate the subcarrier correlation changes in detail.

Specifically, the DTW-based subcarrier selection algorithm includes four steps, i.e., subcarrier sequence correlation calculation, generation of correlation coefficient matrix, subcarrier selection, and frequency spatial considerations.

1) Subcarrier Sequence Correlation Calculation: Since the correlation measurement of the subcarrier sequence is the key to select subcarriers, we start a brief introduction of DTW as follow:

DTW is used for measuring the similarity between two time sequences [33], which may vary in time or speed, and the principle of DTW is to compare two dynamic patterns and measure their similarity by calculating a minimum distance between them. Suppose we have two time sequences $\boldsymbol{V}$ and $\boldsymbol{G}$, which have the length of α and β respectively, where:

$$\boldsymbol{V} = \{v_1, v_2, \ldots, v_i, \ldots, v_\alpha\} \tag{9}$$

$$\boldsymbol{G} = \{g_1, g_2, \ldots, g_k, \ldots, g_\beta\} \tag{10}$$

To align the two sequences using DTW, an $\alpha \times \beta$ matrix is constructed at first, where the (i^{th}, k^{th}) element of the matrix contains the distance $d(t_i, g_k)$ between the two points v_i and g_k. Next, the absolute distance between the values of two sequences is calculated using the Euclidean distance.

$$d(v_i, g_k) = (v_i - g_k)^2 \tag{11}$$

Each element of the matrix (i, k) corresponds to the alignment between the points v_i and g_k. Finally, the accumulated distance is measured by:

$$D(i, k) = \min[D(i-1, k-1), D(i-1, k), D(i, k-1)] + d(i, k) \tag{12}$$

The DTW distance $D(\alpha, \beta)$ obtained by the above formula can represent the correlation of two sequences ($\boldsymbol{V}$ and $\boldsymbol{G}$). Thus, we use the DTW distance to measure the correlation between subcarrier sequences in all sliding windows.

2) Generation of Correlation Coefficient Matrix: Since a longer DTW distance means a smaller correlation coefficient between two subcarriers, the correlation matrix of the f^{th} sliding window can be generated by calculating the DTW distances between different subcarriers. Specifically, for each of the two subcarrier sequences in the f^{th} sliding window, we calculate the

TABLE I
EXPLANATION FOR EXTRACTED FEATURES

Domain	Features	Description or Calculation	Domain	Features	Description or Calculation
Time	Mean	Mean of CSI	Frequency	Normalized-entropy	The disorder of CSI
	Variance	Variance of CSI			$-\sum_{i=1}^{Z/2} FFT_i \cdot \log_2(FFT_i)$
	Max	The highest value of CSI			Z : window size, FFT_i : FFT coefficients
	Min	The lowest value of CSI		Spectrum energy	Frequency domain energy
	Median	Median of CSI			$\sum_{i=1}^{Z/2} FFT_i^2$
	First quantile	First quantile of CSI			Z : window size, FFT_i : FFT coefficients
	Third quantile	Third quantile of CSI		Maximum frequency	Maximum frequency of CSI

DTW distance to represent the correlation coefficient between these two subcarriers. Then, the correlation matrix $Dist_f$ of the f^{th} sliding window is generated, and the element $Dist_f(\boldsymbol{q}, \boldsymbol{w})$ in $Dist_f$ represents the DTW distance between the subcarrier sequence $\boldsymbol{q}$ and the subcarrier sequence $\boldsymbol{w}$. Similarly, the same operation is performed for each sliding window. Thus, the correlation coefficient matrices for all sliding windows are generated.

To prevent a too large or too small weight of a sliding window in the whole samples, and prevent outliers and extreme values. The correlation matrices $Dist$ in each sliding window need to be normalized. The normalization formula is expressed as:

$$Distnor(\boldsymbol{q}, \boldsymbol{w}) = \frac{Dist(\boldsymbol{q}, \boldsymbol{w}) - \min(Dist)}{\max(Dist) - \min(Dist)} \tag{13}$$

where $Dist$ is the correlation matrix of the sliding window, and $\max(Dist)$ and $\min(Dist)$ are the maximum and minimum values of the matrix $Dist$, respectively. $Distnor$ is a normalized correlation matrix in the same sliding window.

After the normalization of each sliding window correlation matrix, the DTW-based algorithm selects subcarriers from the total subcarrier correlation matrix $Distnor\_total$ generated by adding normalized correlation matrices $Distnor$ of all sliding windows.

3) Subcarrier Selection: After getting the total correlation matrix $Distnor\_total$, the two subcarriers with the weakest correlation are chosen from matrix $Distnor\_total$ to form the subcarrier combination C_{tmp} at first. Then, subcarriers are gradually added to the subcarrier combination C_{tmp} according to the weakest total correlation (the longest total DTW distance) until the number of subcarriers in C_{tmp} reaches the given value o (the expected number of selected subcarriers). Thus, the output subcarrier combination of this step C_{tmp} is determined.

4) Frequency Spatial Considerations: Similarly, the subcarriers in C_{tmp} should also satisfy the frequency spatial constraint and be selected from all three intervals, which are [0, 10), [10, 20), and [20, 30]. If C_{tmp} does not satisfy this constraint, the second weakest correlated subcarrier combination is chosen as the final selected subcarrier combination C_s. Besides, if the second weakest correlated subcarrier combination does not satisfy the condition, the third weakest correlated subcarrier combination is chosen, and so on.

F. Data Preprocessing, Feature Extraction, and Classification

Data preprocessing achieves the glitch filtering of raw signals and the segmentation of motion samples. Two steps are included in this part. Firstly, the weighted moving average [34] is used to smooth the CSI signals. Secondly, the sliding windows over data streams are used to segment the motion samples.

According to the features list in Table I, we extract 10 statistic features from both time and frequency domain, which are widely used in CSI-based HAR systems [7]–[9], [11], [18], [19].

To evaluate the performance with different classifiers, six classical classification methods are used to recognize activities, which are the Random Forest (RF), the Decision Tree (DT), the Decision Tree Regression (DR), the k-NearestNeighbor (kNN), the Logistic Regression (LR) and the Linear Discriminant Analysis (LDA).

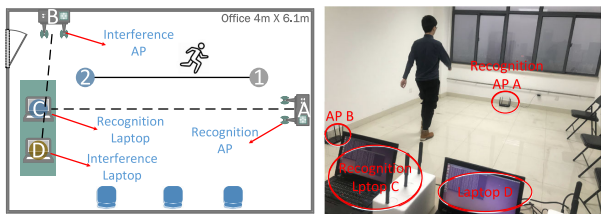

(a) (b)

Fig. 8. Evaluation scenarios in a conference room. (a) The schematic diagram. (b) Experimental setting.

V. EXPERIMENTAL EVALUATION

This section illustrates the implementation and experimental evaluation of WiAnti. Firstly, experimental settings are introduced. Then, the CCI assessment is presented. Next, the performance of WiAnti-Pearson and other pioneer algorithms in the same constant CCI scenario is given. Besides, the performance of WiAnti-DTW and other algorithms in the same scenario with varying CCI is presented. Finally, the impact of various factors on each algorithm performance is demonstrated through experiments.

A. Implementation

As shown in Fig. 8, the experiment is conducted in a 6.1 m $\times$ 4 m room, which contains a table and chairs for daily use. The distance between point 1 and point 2 is 3 m. The distance between laptop C and laptop D is 30 cm. Router A and laptop C are placed in opposite positions. To verify the robustness of our algorithms to the CSI collection NICs, we choose two NICs, i.e., Intel 5300 NIC [8] and Atheros 9580 NIC [24] for CSI data collection. Table II shows the specific settings for different equipment in Fig. 8. The model of laptops

TABLE II
SPECIFIC SETTINGS FOR DIFFERENT CSI COLLECTION NICS

Collect CSI NICs	Tools	A	B	C	D
Intel 5300	CSITOOL	Tp-Link Router	Tp-Link Router	Laptop-Intel 5300	Laptop-Intel 5300
Atheros 9580	Atheros-CSI-Tool	Laptop-Atheros 9580	Tp-Link Router	Laptop-Atheros 9580	Laptop-Intel 5300

is Thinkpad 420i, and the operating system is Ubuntu 14.04 with Linux Kernel 4.1.10. Each laptop (including interference laptops for a fair comparison) is equipped with three 8dBi external antennas to better signal reception. The model of routers is TL-WDR7500V3.0, which contains three 2.4GHz transmit antennas with 5dBi antenna gain.

To measure the impact of constant CCI and varying CCI on CSI, a comparison experiment which includes the scenarios without CCI, with constant CCI, and with varying CCI is performed.

1) Implementation of Non-CCI Scenario: In the scenario without CCI, the access point (AP) A is set to channel 1 and forms a wireless link with the laptop C. AP B and laptop D are powered off. Since the activities such as lifting legs and closing legs during walking or running happen in a few seconds, the beacon rate of the recognition AP A is set to 100 packets per second to capture the signal components affect by these short time activities. Besides, the packet length of AP A is set to the default 64 bytes.

2) Implementation of Constant CCI Scenario: In the constant CCI scenario, AP B is powered on and set to channel 3. The difference of center frequency between channel 3 and channel 1 is 10MHz, and the number of the spectrally-overlapped subcarriers occupies half of all subcarriers. Moreover, Laptop D is powered on and connected to AP B to form a wireless link, and the beacon rate of AP B is set to 100 packets per second. In addition, the packet length of AP B is set to 25000 bytes. Thus, the amount of data generated by interference AP B is about 2.5 Mbytes per second.

3) Implementation of Varying CCI Scenario: In the varying CCI scenario, the interference AP B is adjusted from channels 1 to 5 to produce a varying CCI environment since only the channels 1 to 5 overlap with the channel of the recognition AP A which is set to channel 1.

We perform the comparison experiment on six participants in all of the non-CCI scenario, the constant CCI scenario, and the varying CCI scenario. We also design four different actions, i.e., standing at point 1, walking between point 1 and point 2, running between point 1 and point 2 and sitting at point 1, and a reference state, i.e., the empty room. Each action or state is repeated 54 times for one participant. Thus, a total of $3 \times 6 \times 5 \times 54$ activity samples is collected for training and testing.

B. CCI Assessment

By recording the number of received packets per unit time, the existence and the change of CCI are judged. The impact of subcarrier spectrally-overlap on packet reception is demonstrated by experiments. The data is collected from the constant CCI scenario introduced in Section V-A2, and the channel of interference AP B is changed from 1 to 13.

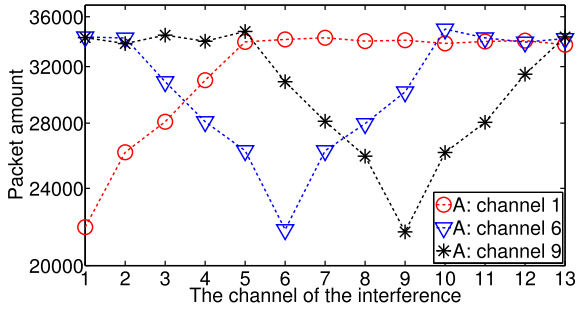

Fig. 9. The number of received packets in six minutes.

Fig. 9 shows the number of packets received by laptop C in six minutes as the channel of interference AP B varies. Each experiment is repeated ten times, taking the average as the number of received packets per unit time. When the channel of the recognition AP A is channel 6, the number of received packets per unit time first decreases rapidly, then rises quickly and finally stabilizes. This is because more overlapped subcarriers caused by the approaching interference channel lead to more severe CCI, which results in the decrease of received packet numbers per unit time. Otherwise, the number of received packets per unit time becomes stable when there are no overlapped subcarriers. Similar results are obtained when we set the recognition AP A to channel 1 and channel 9, respectively.

Built upon the above analysis, by recording the number of received packets per unit time and the sampling frequency, the existence and the change of CCI can be determined. Specifically, the state of the CCI change is judged by Eq. (5) and Eq. (6) as introduced in Section IV-C2. Besides, based on empirical knowledge, the threshold σ in Eq. (5) is set to 0.1 and the threshold ξ in Eq. (6) is set to 0.07.

C. WiAnti's Accuracy

1) Baseline Methods: We compare our subcarrier selection algorithms with two state-of-the-art subcarrier fusion algorithms used by WiFall-1 [19] and WiFall-2 [9]. These two algorithms are widely used in CSI signal data dimension reduction and proved to be effective with less information loss [35]. For a fair comparison with our algorithms, we use the same filtering method to smooth the same original signals, the same sliding window size to realize data segmentation, extract the same features, and use the same classifiers to perform activity classification. Furthermore, the number of selected subcarriers o in our algorithms (except for the algorithm applied to non-CCI scenarios) and all baseline approaches is set to 6 for a fair comparison.

2) Constant CCI Deployments: A Python module *Scikit-learn* [36] as the machine learning library is adopted to quickly

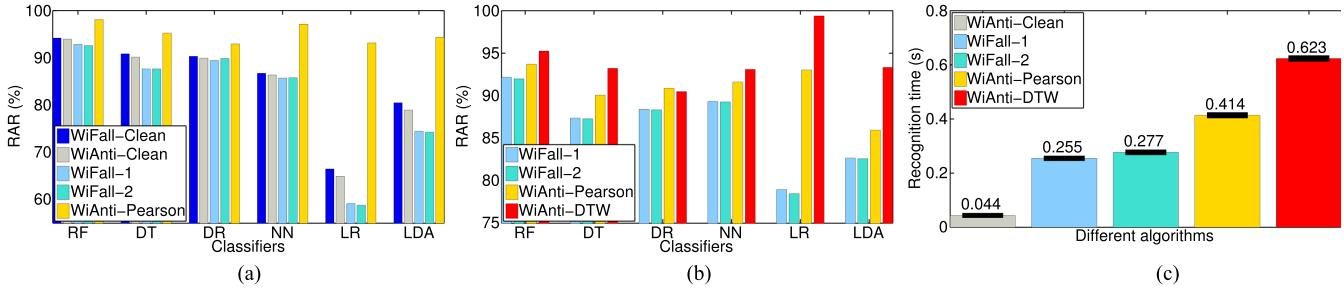

Fig. 10. Comparison of the different algorithm performance, CSI collection tool: CSITOOL. (a) Comparison of different system RARs in the constant CCI scenario under various classifiers. (b) Comparison of different system RARs in the varying CCI scenario under various classifiers. (c) Comparison of various algorithm recognition time for a single motion sample.

implement RF, DT, DR, kNN, LR, and LDA. To avoid overfitting, 10-fold cross-validation is used to train these classifiers. The RAR used in this paper is defined as the ratio of the number of correctly classified activities $\varepsilon_{correct}$ to the number of the whole testing activities ε_{whole}, which can be expressed as follows:

$$RAR = \frac{\varepsilon_{correct}}{\varepsilon_{whole}} \times 100\% \tag{14}$$

Fig. 10(a) shows the RARs of WiAnti algorithms compared with other methods by various classifiers, and WiAnti-Pearson selects $1^{st}, 6^{th}, 16^{th}, 23^{rd}, 29^{th}, 30^{th}$ subcarriers in the constant CCI scenario. As reference states of the non-CCI environment (only recognition AP signals can be detected as introduced in Section V-A1), WiFall-Clean and WiAnti-Clean represent the RARs of WiFall-1 and WiAnti (WiAnti uses the subcarrier fusion algorithm as introduced in Fig. 6) in the scenario without CCI, respectively. Besides, the rest of the experiments are performed in the same constant CCI scenario. From Fig. 10(a), we can observe that the proposed WiAnti-Pearson can achieve better performance compared with the baselines in all cases. By six different classifiers testing, WiAnti-Pearson achieves a 95.165% RAR on average, and the RF classifier can obtain the highest RAR of 98.09%. Compared with the WiFall-2, WiAnti-Pearson gets a 13.675% higher RAR in the constant CCI scenario. For the reference state of the non-CCI environment, the performance of WiFall-1 (represented by the WiFall-Clean) has a significant improvement compared with the same algorithm in the constant CCI scenario. This means that the performance of the pioneer subcarrier fusion algorithm is indeed affected by CCI. Although only one subcarrier data are used, WiAnti-Clean achieves similar performance with WiFall-Clean, and the RAR is enough for WiAnti to classify activity accurately due to the strong subcarrier correlation in the non-CCI environment. Furthermore, WiAnti-Pearson applied in the constant CCI scenario, gets a 3.89% higher RAR than WiFall-Clean, which clearly means by considering the correlation effect in the process of subcarrier selection, the Pearson-based approach is suitable for the task of HAR with WiFi signals when the CCI exists.

Then, two confusion matrices using NN as a classifier are illustrated to demonstrate the robustness of the algorithms to similar actions in the constant CCI scenario. The similar motions for our system are walking and running. The horizontal

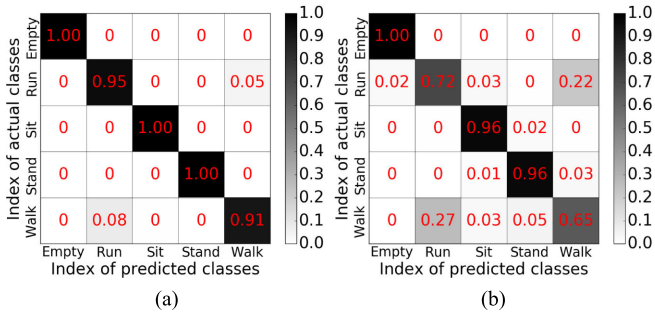

Fig. 11. Confusion matrix for different systems. (a) WiAnti-Pearson uses NN. (b) WiFall-2 uses NN.

coordinates of Fig. 11 represent the type of predicted actions, and the vertical coordinates represent the actual type of actions. The indexes 1 to 5 represent the empty room, running, sitting, standing, and walking, respectively. From Fig. 11(a), we can observe that WiAnti-Pearson is capable of recognizing similar activities with a low error rate in the constant CCI scenario. Compared with the confusion matrix of WiFall-2 shown in Fig. 11(b), WiAnti-Pearson can classify normal actions, i.e., empty rooms, sitting, standing, with high RARs close to 100%. Furthermore, WiAnti-Pearson achieves a 93% RAR of the similar activities, i.e., walking and running. In contrast, Fig. 11(b) depicts that WiFall-2 achieves high RARs of normal activities. However, CCI has quite a significant impact on similar activity RARs. Thus, compared with the WiFall-2, WiAnti-Pearson is more robust to the similar action classification in the constant CCI scenario.

3) Varying CCI Deployments: We also examine the performance of different algorithms in the scenario with varying CCI. Specifically, WiAnti-Pearson and WiAnti-DTW choose $2^{nd}, 6^{th}, 16^{th}, 21^{st}, 26^{th}, 28^{th}$ subcarriers and $1^{st}, 6^{th}, 14^{th}, 16^{th}, 26^{th}, 29^{th}$ subcarriers in the varying CCI scenario, respectively. Fig. 10(b) shows the experimental results of different algorithms in the varying CCI scenario. We observe that the proposed WiAnti algorithms consistently outperform WiFall-1 and WiFall-2 in terms of RAR. Since the varying CCI environment for each algorithm is consistent, a higher RAR means a better ability to maintain motion information. Among WiAnti algorithms, the proposed DTW-based subcarrier selection algorithm can achieve the best performance, reaching

TABLE III
RESULTS FOR WIANTI-DTW

Classes	RAR	Recall	F1 Score
Empty	100%	100%	100%
Running	97.87%	99.38%	98.62%
Sitting	100%	100%	100%
Standing	99.69%	98.77%	99.22%
Walking	99.38%	98.77	99.07%

TABLE IV
RESULTS FOR WIFALL-2

Classes	RAR	Recall	F1 Score
Empty	80.85%	88.58%	84.54%
Running	71.43%	67.90%	69.62%
Sitting	81.06%	89.81%	85.21%
Standing	87.22%	71.60%	78.64%
Walking	72.59%	74.38%	72.48%

a 94.125% RAR on average. By using DTW to measure the correlation between subcarriers, the WiAnti-DTW can significantly increase the representation of selected subcarriers. Moreover, by effective integration of all sling window correlations, WiAnti-DTW can minimize the loss of information under CCI and is suitable for the task of HAR under CCI environment even when the CCI is varying.

To further evaluate the performance of different algorithms in the varying CCI scenario, the comparison tables of the RAR, the recall rate, and the F1 score for WiAnti-DTW and WiFall-2 are presented. The classifier used by the two algorithms is LR. Table III shows that WiAnti-DTW can classify not only all motions with high RARs but also achieves high recall rates and F1 scores. Moreover, Wianti-DTW achieves a 98% similar activity RAR on average with a high recall rate reaching 99%. Therefore, WiAnti-DTW is suitable and reliable for similar action classification in the scenario with varying CCI.

4) Recognition Speed: Fig. 10(c) depicts the recognition time of a single motion sample for different algorithms, including the time of signal processing, feature extraction, and classification. Since only one subcarrier is used, WiAnti-Clean realizes 6× faster on average than WiFall algorithms, and the RAR of WiAnti-Clean is satisfactory in the non-CCI scenario due to the strong correlation between subcarriers. Although the recognition time of WiAnti-Pearson and WiAnti-DTW is longer than that of WiFall algorithms, the improvement of recognition performance in CCI scenarios is significant. Moreover, since the motions usually last several seconds, the increased extra time (0.3s on average) of WiAnti algorithms for HAR systems is tolerable.

D. Deep Dive Into WiAnti

The primary purpose of this section is to understand the impact of various factors on different algorithm performance. The RAR of this part is the average RAR of the six classifiers. Similar to the implementation of the varying CCI scenario as introduced in Section V-A3, the experiment data of each setting value under one factor is collected from 6 participants. For every participant, each action or state is repeated 54 times for each setting value under one factor.

1) Impact of Interference Traffic Rate: In this section, we study the effect of ITR on classification performance. We keep one interference AP (AP B in Fig. 8) and adjust ping rates and packet lengths of the interferer. The combinations of ping rates and packet lengths are 100 packets per second with 1000-bit packet length (average transmission rate 0.1 Mbit/s), 200 packets per second with 5000-bit packet length (average transmission rate 1 Mbit/s), 100 packets per second with 25000-bit packet length (average transmission rate 2.5 Mbit/s), 200 packets per second with 25000-bit packet length (average transmission rate 5 Mbit/s), and 400 packets per second with 20000-bit packet length (average transmission rate 8 Mbit/s). These settings roughly correspond to the bit rates of watching online videos with the frame rates 360p, 480p, and 1080p, which give rise to the bit rates of 1 Mbit/s, 5 Mbit/s, and 8 Mbit/s, respectively. The recognition AP A and the interference AP B are set to channel 1 and channel 3, respectively.

Fig. 12(a) shows the classification performance under different ITRs. WiAnti-Pearson reaches a 93.78% RAR when the ITR is 8 Mbit/s, which means it is robust to the interference generated by people watching the 1080p video. Furthermore, as the interference intensity increases, the RAR of WiAnti-Pearson decreases slowly. Since the subcarrier correlation is considered in the process of selecting subcarriers, WiAnti-Pearson can select the subcarriers which contain more motion information when all the subcarrier correlations are weakened caused by the increasing ITR. In contrast, since there is no anti-interference design, the RARs of WiFall algorithms drop rapidly as the ITR increases. Moreover, the RARs of both WiFall-1 and WiFall-2 are no more than 76% when the ITR is high (8 Mbit/s). Therefore, WiAnti-Pearson is more robust to the increasing ITR and can maintain stability when the ITR is pretty high.

2) Impact of Interference Source Number: To evaluate the impact of the interference source number on classification, we vary the number of interference routers from zero to three. As shown in Fig. 13, we consider four cases: no interference (NONE), one interference AP (AP B), two interference AP (AP B and AP E), and three interference AP (AP B, AP E, and AP F). The recognition AP is set to channel 1, and all interference APs are set to channel 3. The interference laptops also communicate with the corresponding interference APs using the echo request ping command with 100 packets per second ping rate and the 10000-bit packet length (transmission rate 1 Mbit/s).

From Fig. 12(b), compared with two baselines, we can observe that the proposed algorithm WiAnti-Pearson can achieve better performance in different numbers of interference sources. Moreover, the RAR of WiAnti-Pearson drops slowly with the increasing of the interference sources. On the contrary, the RARs of both WiFall-1 and WiFall-2 drop quickly with the increasing of the interference sources. This is because the WiAnti-Pearson can dynamically select suitable subcarriers to cope with the weakened subcarrier correlation caused by the increasing interference sources and maintain more motion information. This also demonstrates that WiAnti-Pearson is more robust to the increasing of the interference sources.

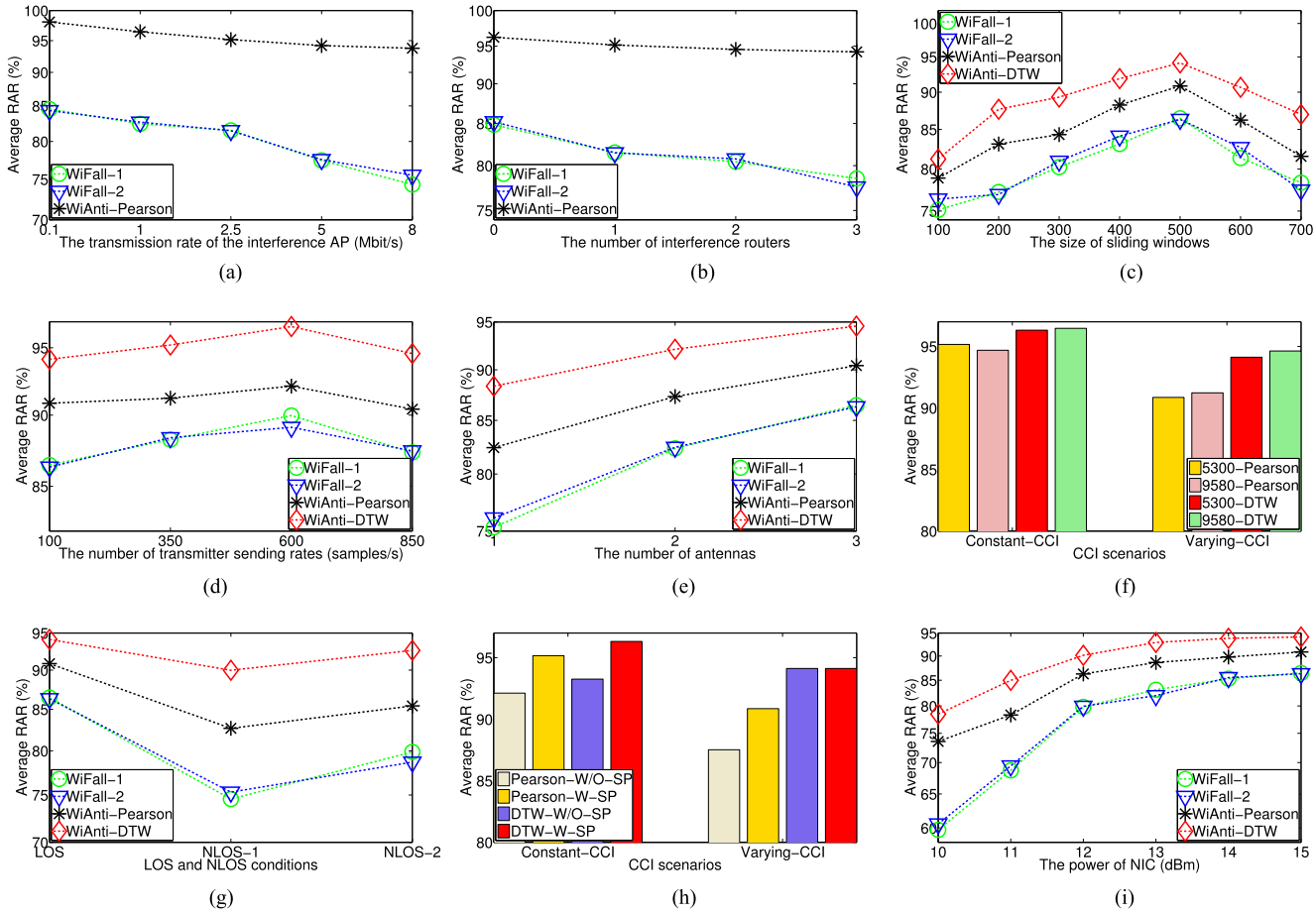

Fig. 12. The impact of various factors on different algorithms. CSI collection tool except (f): CSITOOL. (a) The performance under different interference traffic rates (ITRs). (b) The performance influenced by the number of interference routers. (c) The performance influenced by the size of the sliding window. (d) The performance under different transmitter sending rates. (e) The performance influenced by the number of antennas. (f) The performance influenced by the CSI collection NICs. (g) The performance influenced by the non-line-of-sight (NLOS). LOS: line-of-sight. (h) The performance influenced by the subcarrier frequency spatial constraint. (i) The performance influenced by the power of NIC.

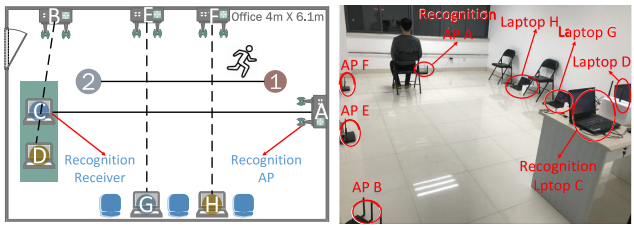

Fig. 13. The location diagram of different interference APs. (a) The schematic diagram. (b) Experimental setting.

3) Impact of Activity Window Size: The activity window size directly affects the accuracy of HAR. Too large window size makes the computational complexity of HAR increase. On the contrary, a too-small window cannot contain all the motion information, and the classification accuracy rate of behavior is reduced accordingly. In order to find the best activity window size, the impact of the window size cw on different algorithm performance is presented. We set cw from 100 to 700, which corresponds to the time difference of $1s$ to $7s$. The experimental data is collected in the scenario with varying CCI introduced in Section V-A3.

Fig. 12(c) depicts that the size of the sliding window has a significant effect on different alforithm RARs. For all algorithms, the performance increases with a larger window size when cw is less than 500 and has a significant drop when cw is large than 500. This is because the 5-second sliding window contains all the motion information, and the shorter sliding window contains less motion information. However, a too-long sliding window cannot guarantee the smoothness of the CSI signals, and the saliency of the motion characteristics can also be affected. Thus, in all the evaluations, we choose 500 as the window size. Regardless of the size of the sliding window, the proposed WiAnti-DTW algorithm can achieve the best performance due to the fact that it can choose the right subcarriers to maximize the contained motion information.

4) Impact of Transmitter Sending Rate: To further evaluate the influence of transmitter sending rate on RARs, we set the four transmitter sending rates of 100 packets/second, 350 packets/second, 600 packets/second, and 850 packets/second. Similarly, the experimental data is collected in the varying CCI scenario introduced in Section V-A3.

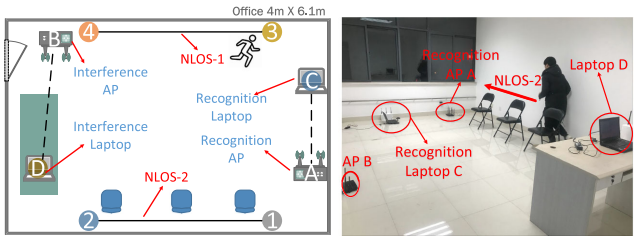

(a) (b)

Fig. 14. The location diagram of different NLOS paths. (a) The schematic diagram. (b) Experimental setting.

From Fig. 12(d), for all algorithms, we observe that the RARs rise with the increasing of the transmitter sending rates and then decrease. This is because setting a higher ping frequency leads to a higher transmitter sending rate of CSI, which ensures that the time resolution of the CSIs is high enough for capturing the maximum details of different types of activities. However, the tool [8] we use to collect CSI signals is not stable at high transmitter sending rates. Thus, the RARs of each algorithm have a slowly decrease when the transmitter sending rate is higher than 600 packets/second. Furthermore, under different transmitter sending rates, the proposed WiAnti-DTW algorithm can always achieve the best performance in the varying CCI scenario.

5) Impact of Antenna Number: In MIMO systems, the number of antennas determines the quality of the signals. To evaluate the influence of antenna numbers on HAR performance, we set up a comparison experiment with three different antenna numbers. Besides, the experimental data of this part is collected in the scenario with varying CCI introduced in Section V-A3.

Fig. 12(e) demonstrates that more antennas at the receiver side can increase the RARs. This is because the use of multiple antennas provides extra diversity gains, especially in the lower CSI strength. As shown in Fig. 12(e), although only one received antenna data are used, the proposed WiAnti-DTW achieves an 88.35% RAR on average. This means WiAnti-DTW is robust to the small number of antennas, and the data from one antenna are enough for WiAnti-DTW to achieve satisfactory recognition performance in the scenario with varying CCI. Furthermore, more antennas make better performance.

6) Impact of CSI Collection NICs: To test the robustness of WiAnti algorithms under different CSI collection devices, as introduced in Section V-A, we also employ Atheros 9580 NIC using Atheros-CSI-TOOL [24] to collect CSIs in the constant and varying CCI scenarios, respectively. Fig. 12(f) depicts the impact of different CSI NICs on WiAnti performance, and we can observe that the performance of our algorithms based on distinct NIC devices is similar and satisfactory in different CCI scenarios, which clearly illustrates that our algorithms are robust to different devices and the WiAnti system does not depend on a specific device platform for implementation.

7) Impact of NLOS Paths: To evaluate the impact of NLOS caused by walls and locations, as shown in Fig. 14, we change the position of the recognition AP A and the recognition laptop C and repeat the various motions on two NLOS paths accordingly. The experiment is conducted in the varying CCI scenario. Fig. 12(g) shows the performance of various algorithms under different NLOS path impact. We can observe that NLOS paths downgrade the performance of each algorithm, and the negative effect is more significant for the path (NLOS-1), which is farther away from the recognition AP. Nevertheless, WiAnti-DTW can always achieve the best performance in all paths. Since more motion information is maintained due to the valid subcarrier selection algorithms, WiAnti is more robust to different NLOS paths and positions.

8) Impact of Frequency Spatial Constraint: To test the impact of the frequency spatial constraint on WiAnti algorithm performance in various CCI scenarios, the RARs of WiAnti algorithms with and without this constraint are given in Fig. 12(h). Fig. 12(h) depicts that the frequency spatial constraint can effectively improve the WiAnti algorithm RARs in most cases due to the consideration of subcarrier frequency responses. In particular, if the selected subcarrier combination initially satisfies the frequency spatial characteristic constraint, i.e., WiAnti-DTW in the varying CCI scenario, the RAR will not be affected by this constraint.

9) Impact of NIC Power: To further evaluate the influence of signal-noise ratio (SNR) on various algorithm performance, we adjust the NIC power of recognition laptop C from 10 dBm to 15 dBm (adjustable range for Intel 5300 NIC in Ubuntu 14.04). The experiment is conducted in the varying CCI scenario. As shown in Fig. 12(i), all algorithm RARs downgrade as the NIC power decreases. However, since more motion information is maintained by the effective subcarrier selection, WiAnti algorithm RARs decrease slowly compared with baselines, and WiAnti-DTW can achieve the best performance in all cases. Moreover, when the NIC power is lower than 11 dBm, the baselines no longer recognize motion accurately, but WiAnti works relatively well. Thus, compared with baselines, WiAnti is more robust to the low transmit NIC power. Furthermore, higher NIC power makes better recognition performance.

VI. Conclusion

In this paper, we propose an anti-interference CSI-based HAR system WiAnti. The core of WiAnti is two dynamic subcarrier selection algorithms, which are WiAnti-Pearson and WiAnti-DTW. Especially, by dynamic selecting weakly correlated subcarriers without fusion in CCI scenarios, the proposed algorithms can maintain motion information at the maximum level during the data dimension reduction. Extensive experiments have been performed in different CCI scenarios. Compared with the state-of-the-art baseline algorithms, WiAnti-Pearson can improve the recognition performance by 14% on average in the constant CCI scenario, and WiAnti-DTW achieves an 8% higher RAR on average in the scenario with varying CCI.

References

[1] O. D. Lara and M. A. Labrador, "A survey on human activity recognition using wearable sensors," *IEEE Commun. Surveys Tut.*, vol. 15, no. 3, pp. 1192–1209, Jul.–Sep. 2013.

[2] W. Zhu, J. Hu, G. Sun, X. Cao, and Y. Qiao, "A key volume mining deep framework for action recognition," in *Proc. IEEE Conf. Comput. Vision Pattern Recognit.*, 2016, pp. 1991–1999.

[3] L. Xia and J. K. Aggarwal, "Spatio-temporal depth cuboid similarity feature for activity recognition using depth camera," in *Proc. IEEE Conf. Comput. Vision Pattern Recognit.*, 2013, pp. 2834–2841.
[4] G. Laput and C. Harrison, "Sensing fine-grained hand activity with smartwatches," in *Proc. CHI Conf. Human Factors Comput. Syst*. ACM, 2019, pp 1–13.
[5] S. G. Trost, D. Cliff, M. Ahmadi, N. Van Tuc, and M. Hagenbuchner, "Sensor-enabled activity class recognition in preschoolers: Hip versus wrist data," *Medicine Sci. Sports Exercise*, vol. 50, no. 3, pp. 634–641, 2018.
[6] M. Hassenzahl and N. Tractinsky, "User experience-a research agenda," *Behaviour Inf. Technol.*, vol. 25, no. 2, pp. 91–97, 2006.
[7] Y. Wang, J. Liu, Y. Chen, M. Gruteser, J. Yang, and H. Liu, "E-eyes: Device-free location-oriented activity identification using fine-grained wifi signatures," in *Proc. 20th Annu. Int. Conf. Mobile Comput. Netw*. ACM, 2014, pp. 617–628.
[8] D. Halperin, W. Hu, A. Sheth, and D. Wetherall, "Tool release: Gathering 802.11 n traces with channel state information," *ACM SIGCOMM Comput. Commun. Rev.*, vol. 41, no. 1, pp. 53–53, 2011.
[9] Y. Wang, K. Wu, and L. M. Ni, "Wifall: Device-free fall detection by wireless networks," *IEEE Trans. Mobile Comput.*, vol. 16, no. 2, pp. 581–594, Feb. 2017.
[10] Y. Gu, F. Ren, and J. Li, "Paws: Passive human activity recognition based on wifi ambient signals," *IEEE Internet Things J.*, vol. 3, no. 5, pp. 796–805, Oct. 2016.
[11] H. Abdelnasser, M. Youssef, and K. A. Harras, "Wigest: A ubiquitous wifi-based gesture recognition system," in *Proc. Conf. Comput. Commun. (INFOCOM)*, 2015, pp. 1472–1480.
[12] S. Sigg, S. Shi, F. Buesching, Y. Ji, and L. Wolf, "Leveraging rf-channel fluctuation for activity recognition: Active and passive systems, continuous and rssi-based signal features," in *Proc. Int. Conf. Adv. Mobile Comput. Multimedia*. ACM, 2013, pp 43–52.
[13] N. Xiao, P. Yang, Y. Yan, H. Zhou, and X.-Y. Li, "Motion-fi: Recognizing and counting repetitive motions with passive wireless backscattering," in *Proc. IEEE INFOCOM Conf. Comput. Commun.*, 2018, pp. 2024–2032.
[14] K. Benkic, M. Malajner, P. Planinsic, and Z. Cucej, "Using RSSI value for distance estimation in wireless sensor networks based on zigbee," in *Proc. IWSSIP 15th Int. Conf. Syst., Signals Image Process.*, 2008, pp. 303–306.
[15] W. Xi *et al.*, "Electronic frog eye: Counting crowd using wifi," in *Proc. IEEE Infocom*, 2014, pp. 361–369.
[16] "Ieee standard for information technology," *IEEE Std 802.11n-2009*, pp. 1–565, Oct. 2009.
[17] F. Adib, "See through walls with Wi-Fi," Ph.D. dissertation, Massachusetts Inst. Technol., Electrical Engineering and Computer Science, Cambridge, MA, USA, 2013.
[18] Y. Zeng, P. H. Pathak, and P. Mohapatra, "Analyzing shopper's behavior through wifi signals," in *Proc. 2nd Workshop Physical Analytics*. ACM, 2015, pp. 13–18.
[19] C. Han, K. Wu, Y. Wang, and L. M. Ni, "Wifall: Device-free fall detection by wireless networks," in *Proc. IEEE INFOCOM Conf. Comput. Commun.*, 2014, pp. 271–279.
[20] Y. Zeng, D. Wu, R. Gao, T. Gu, and D. Zhang, "Fullbreathe: Full human respiration detection exploiting complementarity of CSI phase and amplitude of wifi signals," *Proc. ACM Interactive, Mobile, Wearable Ubiquitous Technologies*, vol. 2, no. 3, pp 1–19, 2018.
[21] W. Wang, A. X. Liu, M. Shahzad, K. Ling, and S. Lu, "Understanding and modeling of wifi signal based human activity recognition," in *Proc. 21st Annu. Int. Conf. Mobile Comput. Netw*. ACM, 2015, pp. 65–76.
[22] N. Yu, W. Wang, A. X. Liu, and L. Kong, "Qgesture: Quantifying gesture distance and direction with wifi signals," *Proc. ACM Interactive, Mobile, Wearable Ubiquitous Technologies*, vol. 2, no. 1, pp 1–23, 2018.
[23] K. Ali, A. X. Liu, W. Wang, and M. Shahzad, "Recognizing keystrokes using wifi devices," *IEEE J. Sel. Areas Commun.*, vol. 35, no. 5, pp. 1175–1190, May 2017.
[24] Z. Li, Y. Xie, M. Li, and K. Jamieson, "Recitation: Rehearsing wireless packet reception in software," in *Proc. 21st Annu. Int. Conf. Mobile Comput. Netw*. ACM, 2015, pp. 291–303.
[25] S. Sen, R. R. Choudhury, and S. Nelakuditi, "CSMA/CN: Carrier sense multiple access with collision notification," *IEEE/ACM Trans. Netw.*, vol. 20, no. 2, pp. 544–556, Apr. 2012.
[26] H. Zhang, Y. Ma, D. Yuan, and H.-H. Chen, "Quality-of-service driven power and sub-carrier allocation policy for vehicular communication networks," *IEEE J. Sel. Areas Commun.*, vol. 29, no. 1, pp. 197–206, Jan. 2010.
[27] A. V. Adamis, K. N. Maliatsos, and P. Constantinou, "Methods for reducing interference caused to licensed systems by overlay-CSMA/CA cognitive radios," in *Proc. IEEE 3rd Int. Conf. Cogn. Radio Oriented Wireless Netw. Commun. (CrownCom)*, 2008, pp. 1–6.
[28] G. Bansal, Md J. Hossain, V. K. Bhargava, and T. Le-Ngoc, "Subcarrier and power allocation for OFDMA-based cognitive radio systems with joint overlay and underlay spectrum access mechanism," *IEEE Trans. Veh. Technol.*, vol. 62, no. 3, pp. 1111–1122, Mar. 2013.
[29] S. Singh, M. Shahbazi, K. Pelechrinis, K. Sundaresan, S. V. Krishnamurthy, and S. Addepalli, "A case for adaptive sub-carrier level power allocation in OFDMA networks," in *Proc. 13th ACM Int. Symp. Mobile Ad Hoc Netw. Comput*. ACM, 2012, pp. 225–234.
[30] A. Djouama, E. Zöchmann, S. Pratschner, M. Rupp, and F. Yo. Ettoumi, "Predicting csi for link adaptation employing support vector regression for channel extrapolation," in *Proc. 20th Int. ITG Workshop Smart Antennas*. VDE, 2016, pp. 1–7.
[31] J. Benesty, J. Chen, Y. Huang, and I. Cohen, "Pearson correlation coefficient," in *Noise Reduction in Speech Processing*, Berlin, Germany: Springer, 2009, pp. 1–4.
[32] T. M. Cover and J. A. Thomas, *Elements of Information Theory*, Hoboken, NJ, USA: Wiley, 2012.
[33] L. Muda, M. Begam, and I. Elamvazuthi, "Voice recognition algorithms using mel frequency cepstral coefficient (MFCC) and dynamic time warping (DTW) techniques," 2010, *arXiv:1003.4083*.
[34] J S. Hunter, "The exponentially weighted moving average," *J. Quality Technol.*, vol. 18, no. 4, pp. 203–210, 1986.
[35] S. Yousefi, H. Narui, S. Dayal, S. Ermon, and S. Valaee, "A survey on behavior recognition using wifi channel state information," *IEEE Commun. Mag.*, vol. 55, no. 10, pp. 98–104, Oct. 2017.
[36] F. Pedregosa *et al.*, "Scikit-learn: Machine learning in Python," *J. Mach. Learn. Res.*, vol. 12, pp. 2825–2830, 2011.

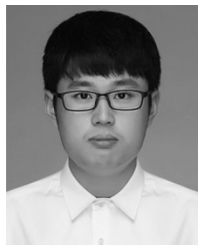

Jinyang Huang received the B.Eng. degree from Anhui University, China in 2017. He is currently working toward the Ph.D. degree with the School of Cyberspace Security from the University of Science and Technology of China. His research interests lie human-computer interaction, wireless sensing, wireless communication, and machine learning.

Bin Liu received the B.S. and M.S. degrees, from the University of Science and Technology of China, Hefei, Anhui, China, in 1998 and 2001, respectively, and the Ph.D. degree from Syracuse University, Syracuse, NY, in 2006, all in electrical engineering, Currently, he is an Associate Professor with the School of Information Science and Technology, University of Science and Technology of China. His research interests are signal processing and communications in wireless sensor and body area networks.

Chao Chen received the B.Eng. degree from Anhui University, China in 2016. He is working toward the Ph.D. degree with the School of Information Science and Electrical Engineering, Zhejiang University, China. Currently, he is Visiting the University of California, Los Angeles (UCLA) sponsored by China Scholarship Council. His research interests include statistics and optimization, deep learning and transfer learning.

Hongxin Jin received the B.S. and M.S. degrees, from the University of Science and Technology of China, Hefei, Anhui, China, in 2015 and 2018, respectively both in electrical engineering, Currently, he is an Algorithm Engineer, and his research interests are artificial intelligence, neural network, and video analysis.

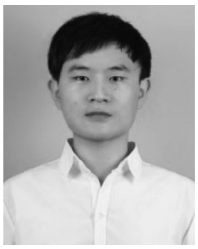

Zhiqiang Liu received the B.S degrees in electrical engineering, in 2013, from the University of Science and Technology of China, Hefei, Anhui, China, where he is currently working toward the Ph.D. degree in electrical engineering. His research interests lie resource allocation, energy-saving and quality of service guarantee in wireless body area networks.

Chi Zhang received the B.E. and M.E. degrees in electrical and information engineering from the Huazhong University of Science and Technology, Wuhan, China, in 1999 and 2002, respectively, and the Ph.D. degree in electrical and computer engineering from the University of Florida, Gainesville, Florida, in 2011. He joined University of Science and Technology of China in September 2011 as an Associate Professor of School of Information Science and Technology. His research interests are in the areas of network protocol design, network performance analysis, and network security guarantee.

Nenghai Yu received the B.S. degree from the Nanjing University of Posts and Telecommunications, in 1987, the M.E. degree from Tsinghua University, in 1992, and the Ph.D. degree from the University of Science and Technology of China, in 2004. He is currently a Professor with the University of Science and Technology of China. His research interests include multimedia security, multimedia information retrieval, video processing, information hiding and security, privacy, and reliability in cloud computing.